Biophysical Journal, Volume *112*

Supplemental Information

Contributions of Microtubule Dynamic Instability and Rotational Diffusion to Kinetochore Capture

Robert Blackwell, Oliver Sweezy-Schindler, Christopher Edelmaier, Zachary R. Gergely, Patrick J. Flynn, Salvador Montes, Ammon Crapo, Alireza Doostan, J. Richard McIntosh, Matthew A. Glaser, and Meredith D. Betterton

Supporting Material

R. Blackwell, O. Sweezy-Schindler, C. Edelmaier, Z. R. Gergely, P. J. Flynn, S. Montes, A. Crapo, A. Doostan, J. R. McIntosh, M. A. Glaser, and M. D. Betterton

I. MODEL

MTs are rigid spherocylinders (cylinders with hemispherical ends) with length $L(t)$ and diameter σ_{MT}. One end of the MT is fixed to a point on the nuclear envelope. The equations of motion for microtubule reorientation are

$$\mathbf{u}_i(t+\delta t) = \mathbf{u}_i(t) + \frac{D_\theta(L)}{k_B T}\mathbf{T}_i(t)\times\mathbf{u}_i(t)\delta t + \delta\mathbf{u}_i(t), \tag{S1}$$

where $D_\theta(L)$ is the rotational diffusion coefficient, $\mathbf{T}_i(t)$ is the systematic torque on particle i, and the random reorientation $\delta\mathbf{u}_i(t)$ is Gaussian-distributed, with variance $\langle\delta\mathbf{u}_i(t)\delta\mathbf{u}_i(t)\rangle = 2D_\theta(L)\left[\mathbf{I}-\mathbf{u}_i(t)\mathbf{u}_i(t)\right]\delta t$. MTs have a length-dependent rotational diffusion coefficient $D_\theta\left(L\right) \sim L^{-3}$. Using the formula for spherocylinder rotational diffusion from Löwen *et al.* [1], we calculated $D_\theta\left(L\right)$ for each timestep of the simulation:

$$D_\theta\left(L(t)\right) = \frac{3k_bT}{\pi\eta(L(t)+1)^3}(\ln a_{MT} - 0.662 + 0.917/a_{MT} - 0.050/a_{MT}^2), \tag{S2}$$

where η is the fluid viscosity, and $a_{MT} = L(t)/\sigma_{MT}$.

The MT minimum length is 4 σ_{MT}. We tested shorter minimum lengths, but found that decreasing below 4 σ_{MT} did not significantly change the capture time; this choice of minimum length makes the simulations more stable.

KCs are spheres with diameter σ_{KC} and diffusion coefficient D_{kc} (table 1) that obey the equation of motion

$$\mathbf{r}_i(t+\delta t) = \mathbf{r}_i(t) + \frac{D_{kc}}{k_B T}\mathbf{F}_i(t) + \delta\mathbf{r}_i(t), \tag{S3}$$

with Gaussian random displacements with variance $\langle\delta\mathbf{r}_i(t)\delta\mathbf{r}_i(t)\rangle = 2D_{kc}\delta t$.

To account for variations in the relative diffusion of KCs and MTs, we defined the MT and KC diffusion coefficients independently (fig. S1). We nondimensionalized the parameters using the reference length σ_{MT} of a MT diameter (25 nm), and the reference diffusion coefficient D_0; these together determine the unit of time $\tau = \sigma_{MT}^2/D_0$. A kinetochore of size 200nm has a diffusion constant of $D_{kc} = 5.9\times10^{-4}$ μm^2 s^{-1}. Using Stokes calculation for D, we see that $D_{kc} = \frac{1}{8}D_0$, yielding $D_0 = 4.72\times10^{-3}$ μm^2 s^{-1}.

A. Boundary interactions

To ensure that MTs and KCs remained within the nuclear envelope, both MT free ends and KCs interacted with the envelope via the Weeks-Chandler-Anderson potential [2]

$$u_{\mathrm{wca,fil}}(r_{\min}) = \begin{cases} 4k_BT\left[\left(\frac{\sigma}{r_{\min}}\right)^{12} - \left(\frac{\sigma}{r_{\min}}\right)^{6}\right] + k_BT, & r_{\min} < 2^{1/6}\sigma \\ 0, & r_{\min} \geq 2^{1/6}\sigma, \end{cases} \tag{S4}$$

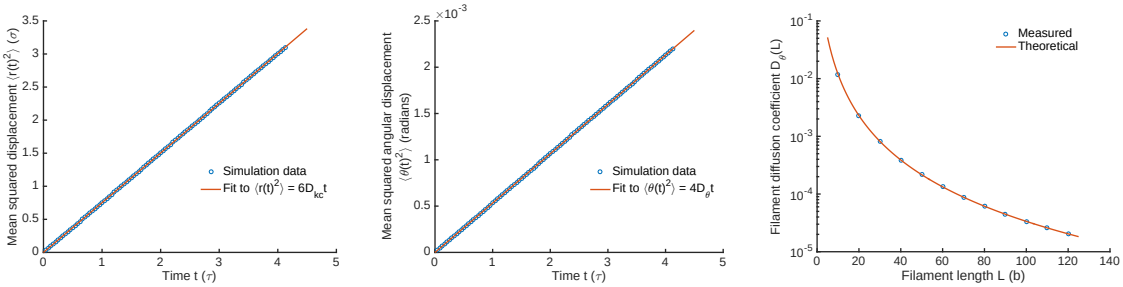

FIG. S1. Diffusion coefficient verification. (a) Kinetochore mean-squared displacement versus time for a 0.2 μm diameter kinetochore. Points indicate measured values from a simulation with no boundary; The line is a linear fit of $\langle r(t)^2\rangle = 6D_{\mathrm{kc}}t$. (b) Filament mean-squared angular displacement versus time. Points indicate measured values from a simulation with no boundary. The line is a linear fit of $\langle \theta(t)^2\rangle = 4D_\theta t$. (c) Rotational diffusion coefficients versus microtubule length for filaments of fixed length. Points are measured values from a simulation with no boundary. The line is the diffusion coefficient from Löwen et al. [1]. Values in all plots are in dimensionless simulation units.

where r_{min} is minimum distance between the free end of the filament and the enclosing sphere with radius $R + \sigma/2$, and σ is the finite distance at which the potential goes to zero. This allows for smooth continuation of the dynamics at the boundary; the nuclear envelope then has an effective radius of R.

Kinetochores have a similar interaction with the envelope

$$u_{\mathrm{wca,kc}}(r_{\mathrm{min}}) = \begin{cases} 4k_BT\left[\left(\frac{\sigma_{\mathrm{kc}}/2+\sigma/2}{r_{\mathrm{min}}}\right)^{12} - \left(\frac{\sigma_{\mathrm{kc}}/2+\sigma/2}{r_{\mathrm{min}}}\right)^{6}\right] + k_BT, & r_{\mathrm{min}} < 2^{1/6}(\sigma_{\mathrm{kc}}+\sigma)/2 \\ 0, & r_{\mathrm{min}} \geq 2^{1/6}(\sigma_{\mathrm{kc}}+\sigma)/2, \end{cases} \tag{S5}$$

where again an enclosing boundary is a sphere with radius $R + \sigma/2$.

B. Dynamic instability models

We consider two dynamic instability models. The first is the original two-state dynamic instability model of Dogterom and Leibler [3]. The microtubule (MT) grows (shrinks) at a constant velocity v_g (v_s), with transition frequencies f_c (f_r) to the other state. This leads to an exponential distribution of MT lengths in the bounded growth regime, with mean length

$$\langle L\rangle = \frac{v_g v_s}{v_s f_c - v_g f_r}. \tag{S6}$$

If the second term in the denominator is small, which commonly occurs in cells when the rescue frequency is low, we have $v_g f_r \ll v_s f_c$ and this becomes approximately

$$\langle L\rangle \approx \frac{v_g}{f_c}. \tag{S7}$$

1. *Slow dynamic instability*

We consider MTs that can be in 3 states: growing, shrinking, or pausing. In the paused state, the MT length doesn't change with time. As in previous work, we consider the probability distribution

of MT state and length $P_s(z,t)$, where s labels the state (+, −, and 0 label growing, shrinking, and pausing states), z length, and t time. The equations of the three-state model are

$$\frac{\partial P_+(z,t)}{\partial t} = -f_{+0}P_+ + f_{0+}P_0 - v_g\frac{\partial P_+}{\partial z}, \tag{S8}$$

$$\frac{\partial P_-(z,t)}{\partial t} = -f_{-0}P_- + f_{0-}P_0 + v_s\frac{\partial P_-}{\partial z}, \tag{S9}$$

$$\frac{\partial P_0(z,t)}{\partial t} = -(f_{0-} + f_{0+})P_0 + f_{+0}P_+ + f_{-0}P_-. \tag{S10}$$

Here f_{+0} is the frequency of transitions from the growing state to the paused state, and so on. To determine the mean length $\langle L\rangle$, we study the steady state equations. After summing the steady state equations, the state switching terms cancel and we have

$$v_+\frac{\partial P_+}{\partial z} = v_-\frac{\partial P_-}{\partial z}. \tag{S11}$$

Integrating both sides of the equation with respect to z and setting the integration constant to 0 (as required for a bounded length distribution for which the probability density goes to zero for large z) gives

$$P_- = \frac{v_+}{v_-}P_+. \tag{S12}$$

Similarly, the steady-state of equation (S10) gives

$$P_0 = \left(\frac{f_{+0} + v_+f_{-0}/v_-}{f_{0+} + f_{0-}}\right)P_+. \tag{S13}$$

Then equation (S8) becomes

$$\frac{\partial P_+}{\partial z} = \left(\frac{-f_{+0}}{v_+} + \frac{f_{0+}f_{+0}}{v_+\left(f_{0+} + f_{0-}\right)} + \frac{f_{0+}f_{-0}}{v_-\left(f_{0+} + f_{0-}\right)}\right)P_+. \tag{S14}$$

If the factor in parentheses on the right side of this equation is negative, then the length distribution is a exponential with mean length

$$\langle L\rangle = \left(\frac{f_{+0}}{v_+} - \frac{f_{0+}f_{+0}}{v_+\left(f_{0+} + f_{0-}\right)} - \frac{f_{0+}f_{-0}}{v_-\left(f_{0+} + f_{0-}\right)}\right)^{-1}. \tag{S15}$$

We consider the case in which transitions from pausing to growing do not occur, so that $f_{0+} = 0$. Then

$$\langle L\rangle = \frac{v_g}{f_{+0}}. \tag{S16}$$

Note the similarity of this expression to equation (S7) with f_{+0} the effective catastrophe frequency of the model.

II. EXPERIMENT

A. Cut7-ts strain construction

Cells were cultured using standard fission yeast techniques [5]. To construct *cut7-ts* strains with mCherry-tagged tubulin, parent strains with the low-expression *mCherry-atb2* MT marker [6]

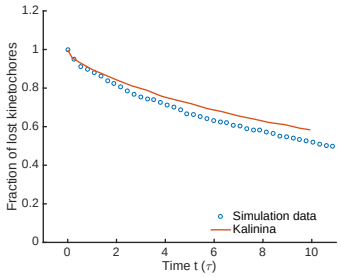

FIG. S2. Comparison of fraction of lost kinetochores versus time in our model to those of Kalinina et al. [4]. For this comparison, we inserted kinetochores in the the nucleus uniformly 1.2 μm from the base of the filament to mimic the approach of Kalinina et al. Microtubules were inserted with uniform angles that did not cause overlap with the boundary. The difference between the two models is likely due to the overlap criteria: Kalinina et al used an approximate angular criterion to detect overlaps that did not account for the non-zero volume of the filament [4]. This effectively decreased the capture radius compared to our model.

and the *cut7-24* allele [7] were crossed on malt extract agar plates. Zygotic asci were isolated by digestion with glusulase (PerkinElmer, Waltham, Massachusetts), counted on a haemocytometer, plated onto YE5S agar plates and allowed to grow into colonies. The colonies were replica plated sequentially onto two different plates, first onto YEP (YE5S plus phloxin B) agar plates. Colonies were allowed to grow at 25°C overnight and then placed at 36°C. After 1-2 days, dark pink colonies indicated dead or dying cells and were selected from the parent plates as being positive for *cut7-24*. Next, colonies were replica plated onto YES + 100 μg/mL nourseothricin (Gold Biotechnology, Olivette, Missouri) agar plates. Candidate colonies that grew were selected as positive for *mCherry-atb2*. Candidates with both *cut7-24* and *mCherry-atb2* were validated by imaging fluorescent MTs in monopolar spindles at 36^{o}C using fluorescence microscopy on an Axioplan II light microscope (Carl Zeiss, Jena, Germany) with a 100x, 1.45 NA Plan Fluor oil-immersion objective, a Bioptechs objective heater (Bioptechs, Butler, PA) and a Photometrics Cascade 650 CCD camera (Roper Scientific, Sarasota, Florida).

B. Measurement of labeled tubulin fraction

A preculture was grown in YPD from which a 50 mL YPD overnight cell culture was grown to late log phase. These cell cultures were pelleted in a tabletop Beckman CS-6 centrifuge, the supernatant was removed, and they were resuspended in 1 mL of NaCl (150 mM)-Tris (50 mM) buffer at pH 8. The cells were washed twice in buffer and resuspended in the same buffer plus 1/2 tablet of complete Mini EDTA-free protease inhibitors (Roche Diagnostics, Mannheim, Germany). The cells were then lysed with a FastPrep FP120 ribolyser (MP Biomedicals, Santa Ana, CA). Lysing tubes were prepared with 1 cm 0.5 μm glass beads on the bottom. 1 mL of cell suspension per tube was lysed on setting 6 for 20 sec for a total of three runs. In between each run, the cells were placed on ice for 10 min. The tubes were spun in a tabletop centrifuge at 5,000 rpm for 6 min and then at 14,000 rpm for 30 min. The clarified lysate was removed and flash frozen with liquid nitrogen.

The cell lysate was mixed 1:1 with Laemmli sample buffer (Bio-Rad, Hercules, CA) plus 5% β-mercaptoethanol. 20 μL samples for ten different lanes were prepared with serial dilutions ranging from 100%-10% of the original cell suspension concentration, and the samples were boiled in water for 7 min. The samples were run on Any KD pre-cast gels in a BioRad Miniprotean II system (Bio-Rad, Hercules, CA) with a Tris (25 mM), glycine (192 mM), 0.1% SDS running buffer. The

Strain	Genotype	Source
Mcl 730	nda3-KM311, cen2::kanr-ura4^{+-}lacOp his7^{+}::lacI-GFP, nmt1-GFP-pcp1^{+}::kanr, mcherry-atb2:natMX6, leu1-32, ura4-D18, h^{-}	This study
McI 804	z:adh15:mcherry-atb2:natMX6, cut7-24, leu1-32, ura4-d18, h^{90}	This study
Original Strains		
McI 728	z:adh15:mcherry-atb2:natMX6, leu1-32, ura4-d18, h^{+}	Y. Wantanabe
McI 789	cut7-24, leu1-32, ura4-d18, h^{+}	I. Hagan

TABLE S1. Fission yeast strains used in this study.

gels were run for 90 min at 100V with ice packs around the gel box.

Immunoblots were then prepared using a modification of standard techniques. Once transfer sandwiches were assembled, samples were transferred to either a nitrocellulose or a PVDF membrane in transfer buffer consisting of Tris (25 mM), glycine (192 mM), 20% methanol, and 0.05% SDS. Blots were run for 1 hr at 80V. The membranes were transferred to a 5% nonfat milk blocking solution in 1x TBS-T (Tris Buffered Saline plus 0.05% Tween 20) and blocked overnight. The blocked membrane was transferred to a sealable bag containing the primary antibody TAT-1 at a 1:1000 dilution for 1 hr at room temperature. The blots were washed 3 times for 15 min in TBS-T and transferred to a sealable bag containing the secondary antibody Goat-anti-Mouse-AP (Bio-Rad, Hercules, CA) at a 1:1000 dilution for 1 hr at room temperature. The blots were washed 3 times for 15 min in TBS-T and transferred to 20 mL of 1-Step NBI/BCIP developing solution (Thermo Scientific, Waltham, MA) for 30 min.

C. Cell preparation for imaging

We grew cells in liquid Edinburgh Minimal Medium (EMM) plus supplements in an overnight preculture, then diluted them over the next 24 hours to keep the cells in mid-exponential growth. Cells were centrifuged at 2,000 rpm for 5 min on a Beckman CS-6 centrifuge (Beckman Coulter, Brea, California). The supernatant was removed and the cells were suspended in 100 μL of EMM filtered with a 0.2 μm filter to reduce background fluorescence from the medium. The solution was placed onto 35 mm no. 1.5 glass bottom dishes (MatTek, Ashland, Massachusetts) coated with 8 μL of 2 mg/mL lectins from *Bandeiraea simplicifolia* (Sigma-Aldrich, St. Louis, Missouri). The cells were allowed to settle and adhere to the lectins for 10 min, then the remaining loose cells were washed away twice with fresh, filtered EMM. 3 mL of fresh, filtered EMM was added to each dish, and the dishes were placed at 36°C.

III. RESULTS

A. Sensitivity analysis

We performed sensitivity analysis to check how the capture time and MT mean length vary with model parameters. As discussed in the main text and above, dynamic instability with no boundary effects gives a mean length of $\langle L\rangle = v_g/f_{+0}$ in the slow model and $\langle L\rangle = v_g v_s/(v_s f_c - v_g f_r) \approx v_g/f_c$ in the fast model. To test these relationships, we performed a global sensitivity analysis of the mean capture time and MT length to the dynamic instability parameters. To quantify this sensitivity, we relied on the analysis of the variance of $\langle\tau_c\rangle$ and $\langle L\rangle$ based on the so-called Sobol' decomposition [8], which we computed directly using the PC expansion [9]. The dynamic instability parameters

Slow model	**Error**
$\langle \tau_c \rangle$ for search and capture	4.9%
$\langle \tau_c \rangle$ with rotational diffusion	3.5%
$\langle L \rangle$ for search and capture	4.4%
$\langle L \rangle$ with rotational diffusion	0.7%
Fast model	
$\langle \tau_c \rangle$ for search and capture	4.6%
$\langle \tau_c \rangle$ with rotational diffusion	3.5%
$\langle L \rangle$ for search and capture	4.4%
$\langle L \rangle$ with rotational diffusion	1.1%

TABLE S2. Error in PC expansion.

were treated as random variables uniformly distributed over the ranges in table 1. The errors from the PC expansion were typically a few percent (ranging from 1-5% depending on which variable and model were fit, table S2). This indicates that the PC expansion is accurately capturing the full simulation results.

The overall contribution of each parameter to the solution variance was quantified using its total Sobol' index [9]; a larger value indicates a higher degree of sensitivity of the model to that parameter (table S3). As expected, $\langle \tau_c \rangle$ and $\langle L \rangle$ are most sensitive to the growth speed and effective catastrophe frequency, and this dependence is not altered significantly by the addition of rotational diffusion to the model.

We also determined the local sensitivity of the capture time to these parameters by computing the gradient (the local direction of steepest change) of $\langle \tau_c \rangle$ as a function of the growth speed and catastrophe frequency from the PC expansion, with other parameters fixed at their reference values (fig. S3 shows results for the models without MT rotational diffusion; here the white line follows the local gradient and passes through the reference parameters). This local sensitivity analysis illustrates the same result found for the global analysis: the capture time is primarily controlled by the growth speed (primarily horizontal arrows in fig. S3) with the main secondary effect from the catastrophe frequency (vertical component of arrows in fig. S3). It also illustrates that the shortest capture times occur for high growth speed and low catastrophe frequency where MT mean lengths are longest.

Total Sobol' indices for slow model	v_g	f_{+0}	v_s	f_{0-}	f_{-0}
$\langle \tau_c \rangle$ for search and capture	**0.74**	**0.32**	1.9×10^{-2}	1.8×10^{-2}	8.9×10^{-3}
$\langle \tau_c \rangle$ with rotational diffusion	**0.70**	**0.39**	9.2×10^{-3}	1.3×10^{-2}	8.0×10^{-3}
$\langle L \rangle$ for search and capture	**0.60**	**0.42**	4.3×10^{-3}	6.5×10^{-3}	3.7×10^{-3}
$\langle L \rangle$ with rotational diffusion	**0.52**	**0.50**	4.0×10^{-4}	2.0×10^{-4}	2.0×10^{-4}
Total Sobol' indices for fast model	v_g	f_c	v_s	f_r	
$\langle \tau_c \rangle$ for search and capture	**0.85**	**0.28**	4.0×10^{-3}	7.5×10^{-3}	
$\langle \tau_c \rangle$ with rotational diffusion	**0.84**	**0.28**	7.3×10^{-3}	9.9×10^{-3}	
$\langle L \rangle$ for search and capture	**0.49**	**0.39**	8.1×10^{-2}	9.5×10^{-2}	
$\langle L \rangle$ with rotational diffusion	**0.50**	**0.39**	7.6×10^{-2}	9.7×10^{-2}	

TABLE S3. Total Sobol' indices.

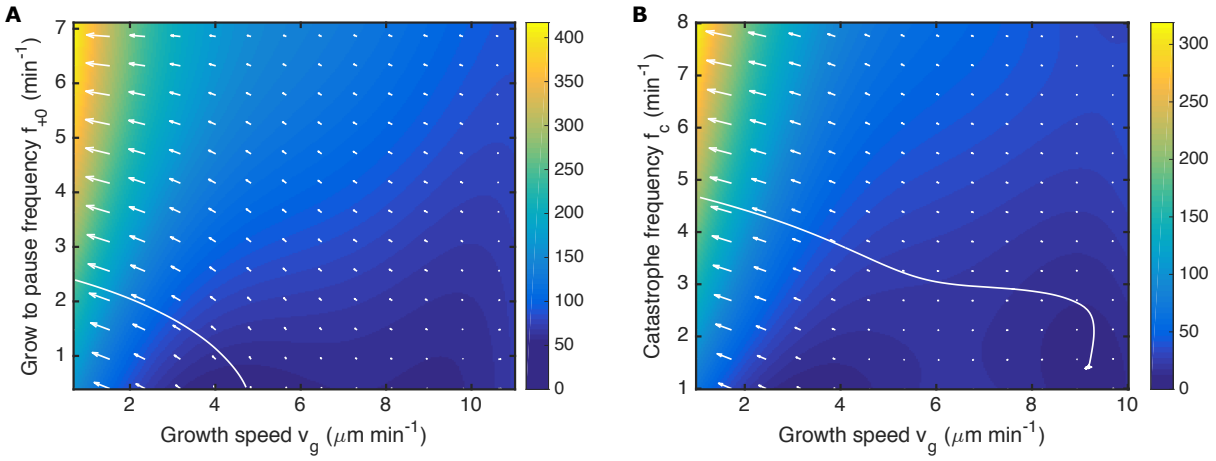

FIG. S3. Dependence of capture time on growth speed and effective catastrophe frequency for search and capture model determined from polynomial chaos expansion. (A) Slow model with no MT rotational diffusion. (B) Fast model with no MT rotational diffusion. Color shows capture time in minutes. White arrows show the magnitude and direction of most rapid change in $\langle \tau_c \rangle$ (the gradient). The white line is the curve that follows the gradient and passes through the reference parameter set.

1. Hartmut Lowen. Brownian dynamics of hard spherocylinders. *Physical Review E*, 50(2):1232–1242, August 1994.
2. John D. Weeks, David Chandler, and Hans C. Andersen. Role of Repulsive Forces in Determining the Equilibrium Structure of Simple Liquids. *The Journal of Chemical Physics*, 54(12):5237–5247, June 1971.
3. Marileen Dogterom and Stanislas Leibler. Physical aspects of the growth and regulation of microtubule structures. *Physical Review Letters*, 70(9):1347–1350, March 1993.
4. Iana Kalinina, Amitabha Nandi, Petrina Delivani, Mariola R. Chacón, Anna H. Klemm, Damien Ramunno-Johnson, Alexander Krull, Benjamin Lindner, Nenad Pavin, and Iva M. Tolić-Norrelykke. Pivoting of microtubules around the spindle pole accelerates kinetochore capture. *Nature Cell Biology*, 2012.
5. Sergio Moreno, Amar Klar, and Paul Nurse. Molecular genetic analysis of fission yeast Schizosaccharomyces pombe. In *Guide to Yeast Genetics and Molecular Biology*, volume Volume 194, pages 795–823. Academic Press, 1991.
6. Y. Yamagishi, C. H. Yang, Y. Tanno, and Y. Watanabe. MPS1/Mph1 phosphorylates the kinetochore protein KNL1/Spc7 to recruit SAC components. *Nature Cell Biology*, 14(7):746–752, 2012.
7. Iain Hagan and Mitsuhiro Yanagida. Novel potential mitotic motor protein encoded by the fission yeast cut7+ gene. *Nature*, 347(6293):563–566, October 1990.
8. I.M. Sobol'. On sensitivity estimation for nonlinear mathematical models. *Matematicheskoe Modelirovanie*, 2(1):112–118, 1990.
9. Bruno Sudret. Global sensitivity analysis using polynomial chaos expansions. *Reliability Engineering and System Safety*, 93(7):964 – 979, 2008.

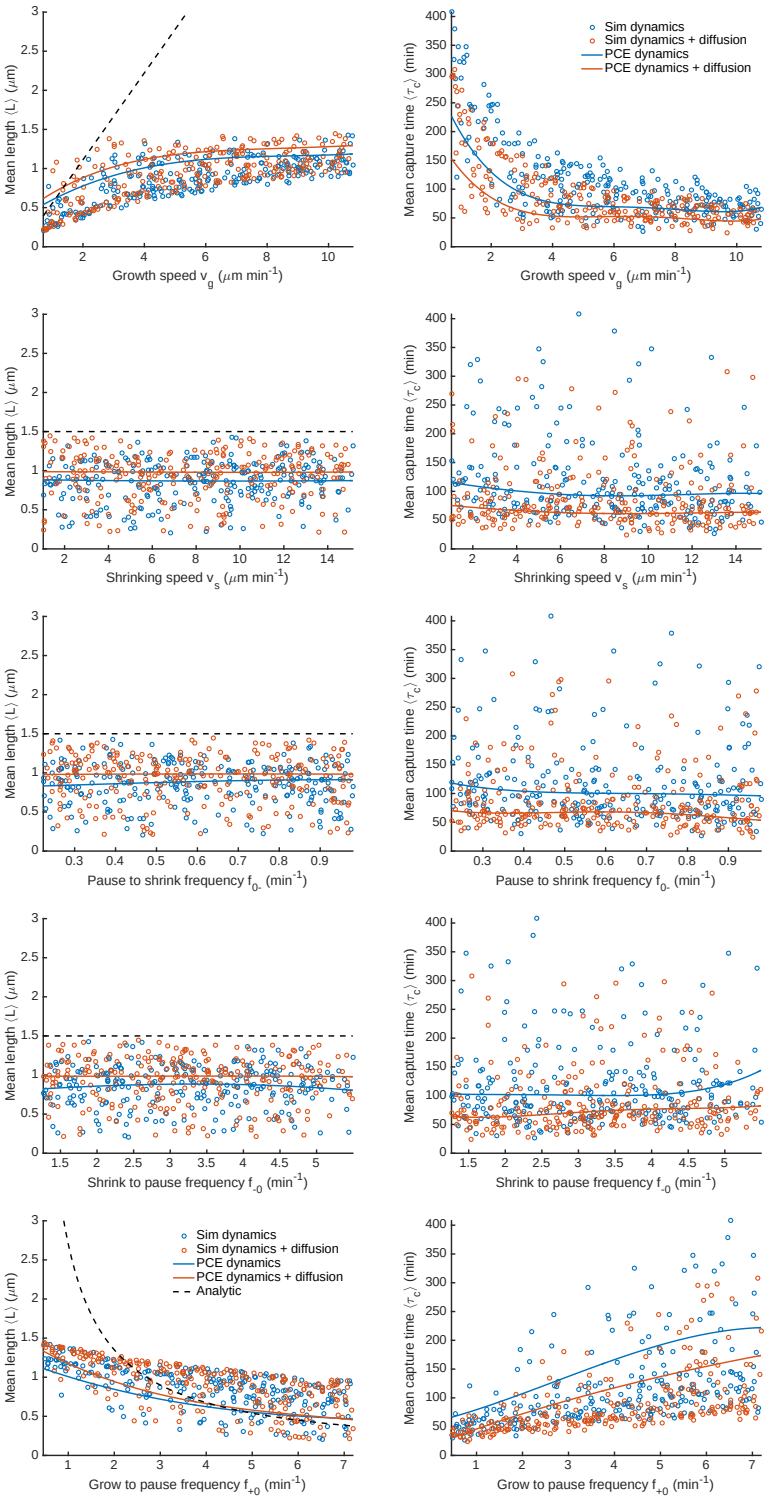

FIG. S4. $\langle L \rangle$ and $\langle \tau_c \rangle$ vs. parameters for slow model.

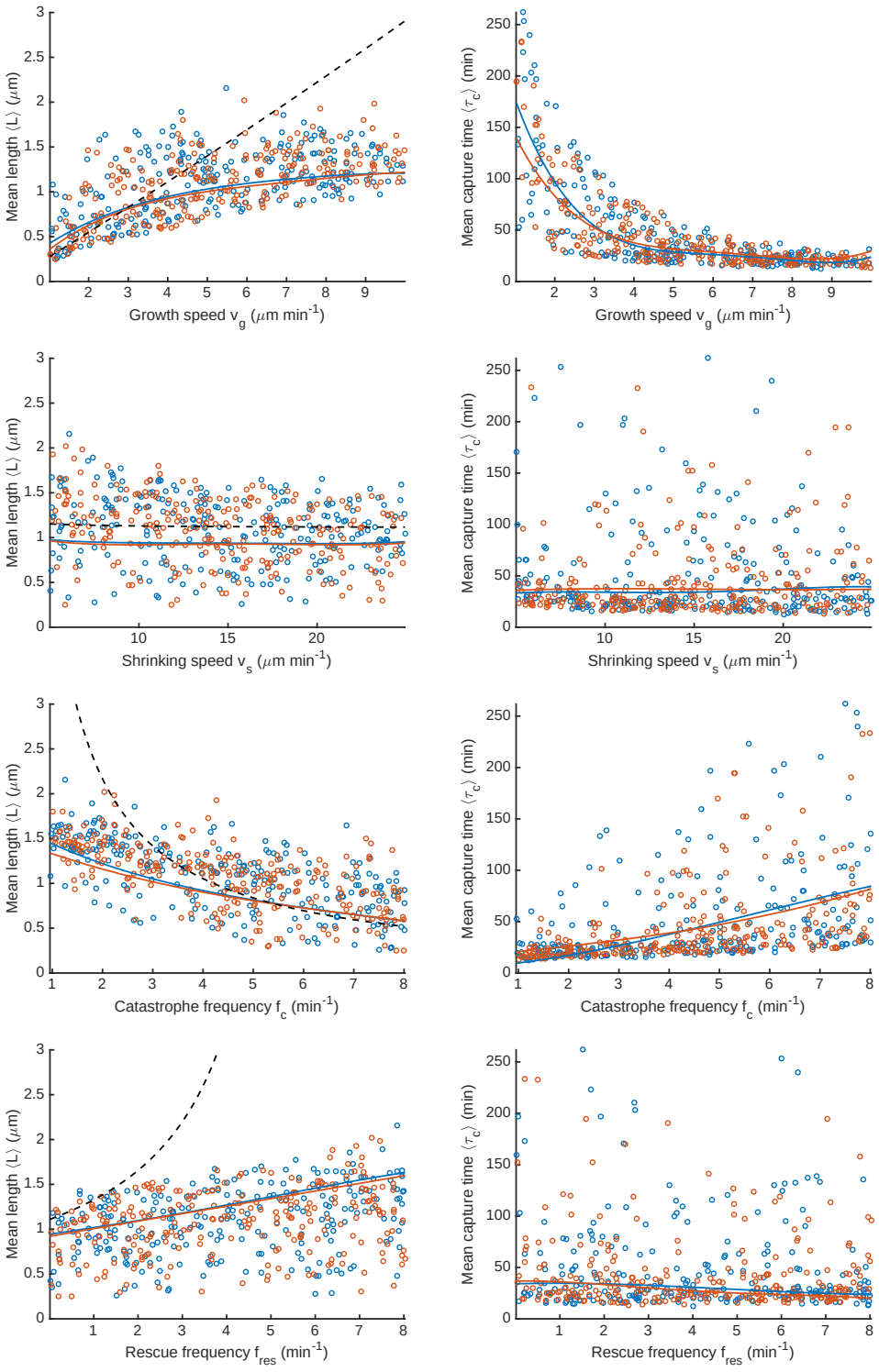

FIG. S5. $\langle L \rangle$ and $\langle \tau_c \rangle$ vs. parameters for fast model.